

Supporting Information for

## Photogenerated Triplet States in Supramolecular Porphyrin Ladder Assemblies: An EPR Study

Sabine Richert,<sup>1</sup> Martin D. Peeks,<sup>2</sup> Claudia E. Tait,<sup>1</sup> Harry L. Anderson,<sup>2\*</sup> and Christiane R. Timmel<sup>1\*</sup>

<sup>1</sup> *Centre for Advanced Electron Spin Resonance (CAESR), Department of Chemistry, University of Oxford, South Parks Road, Oxford, OX1 3QR, United Kingdom.*

<sup>2</sup> *Chemistry Research Laboratory, Department of Chemistry, University of Oxford, Mansfield Road, Oxford, OX1 3TA, United Kingdom.*

\* E-mail: christiane.timmel@chem.ox.ac.uk; harry.anderson@chem.ox.ac.uk

### Table of Contents

<b>1</b>	<b>Experimental Details</b>	<b>S3</b>
1.1	Sample Preparation . . . . .	S3
1.2	Transient cw EPR and ENDOR . . . . .	S3
<b>2</b>	<b>Additional Data and Simulations</b>	<b>S4</b>
2.1	Room Temperature UV-vis Titrations . . . . .	S4
2.2	Low Temperature UV-vis Data . . . . .	S5
2.3	Simulation of the TREPR Spectra . . . . .	S7
2.4	Influence of Porphyrin Side Groups . . . . .	S8
<b>3</b>	<b>DFT Calculations</b>	<b>S9</b>
<b>4</b>	<b>Zero-Field Splitting</b>	<b>S10</b>

### List of Figures

S1	Comparison of the UV-vis spectra of <b>P1</b> to <b>P4</b> with those of solutions containing <b>DABCO</b> in stoichiometric amounts for ladder formation. . . . .	S4
S2	Low temperature UV-vis spectra of the ladder complex of <b>P2</b> . . . . .	S5
S3	Low temperature UV-vis spectra of the ladder complexes of <b>P3</b> and <b>P4</b> . . . . .	S5
S4	UV-vis spectra of <b>P3</b> at different temperatures and higher concentration . . . . .	S6
S5	Simulations of the transient cw EPR spectra of <b>P1</b> to <b>P4</b> . . . . .	S7

S6	Simulation of the transient cw EPR spectra of the ladder complexes of <b>P3</b> and <b>P4</b>	S8
S7	Simulation of the transient cw EPR spectrum of <b>P3 THS</b> . . . . .	S8
S8	Visualisation of the ZFS tensor axes and proton HFI tensors of <b>P1</b> and <b>P2</b> . . . . .	S9
S9	Illustration of the relative energies of the zero-field sublevels for $ Z\rangle >  X\rangle >  Y\rangle$ .	S10

## 1 Experimental Details

### 1.1 Sample Preparation

All EPR samples were prepared at a concentration of 50  $\mu\text{M}$  in toluene. The samples were degassed by the freeze-pump-thaw method (three cycles), backfilled with argon and closed with a subseal. For storage in liquid nitrogen the subseal was removed. The frozen samples were directly inserted into the EPR resonator at 20 K for the measurements.

### 1.2 Transient cw EPR and ENDOR

All transient EPR measurements were carried out at X-band frequencies on a Bruker ELEXSYS E680 spectrometer using a Bruker EN 4118X-MD4 resonator. The temperature was held constant at 20 K using a helium gas-flow cryostat. All samples were excited with 5 mJ pulses of 5 ns duration at 532 nm using a Nd:YAG laser operated at a repetition rate of 10 Hz. Before reaching the sample, the excitation light was depolarised.

The transient cw EPR spectra were acquired in direct detection mode using the transient recorder and a microwave power of 0.2 mW. After data acquisition, the 2D spectra were baseline corrected in both dimensions using a home-written MATLAB [1] routine. The spectra shown in the figures have been averaged over a time window from 0.2  $\mu\text{s}$  to 1  $\mu\text{s}$  after laser excitation.

Proton Mims ENDOR spectra were acquired using the pulse sequence  $\frac{\pi}{2} - \tau - \frac{\pi}{2} - T - \frac{\pi}{2} - \tau$  and a microwave pulse length of 16 ns. Between the second and third pulse of the stimulated echo pulse sequence (i.e. during the delay  $T$ ) a 15  $\mu\text{s}$  RF pulse was applied. The RF power was adjusted based on a nutation experiment such that the flip angle corresponded to  $\pi$ . The integrated echo intensity was then monitored as a function of the RF frequency in a range centered about the  $^1\text{H}$  Larmor frequency at the respective field position. For every chosen field position, three spectra with different  $\tau$  values of 120, 180, and 240 ns were recorded to compensate for blind spots and added to yield the spectra shown in the main text.

## 2 Additional Data and Simulations

### 2.1 Room Temperature UV-vis Titrations

To monitor and confirm ladder formation at room temperature, UV-vis titrations of the linear porphyrin oligomers **P1** to **P4** with the bridging ligand **DABCO** were carried out. **Figure S1** shows a comparison of the UV-vis absorption spectra of the free oligomers and those of solutions of the linear oligomers containing **DABCO** in stoichiometric equivalents for ladder formation. Upon addition of **DABCO**, gradual changes can be observed in the UV-vis spectra. For **P1**, no indications for the formation of an intermediate ladder-type complex are present at the employed concentrations due to a comparatively weak association constant [2].

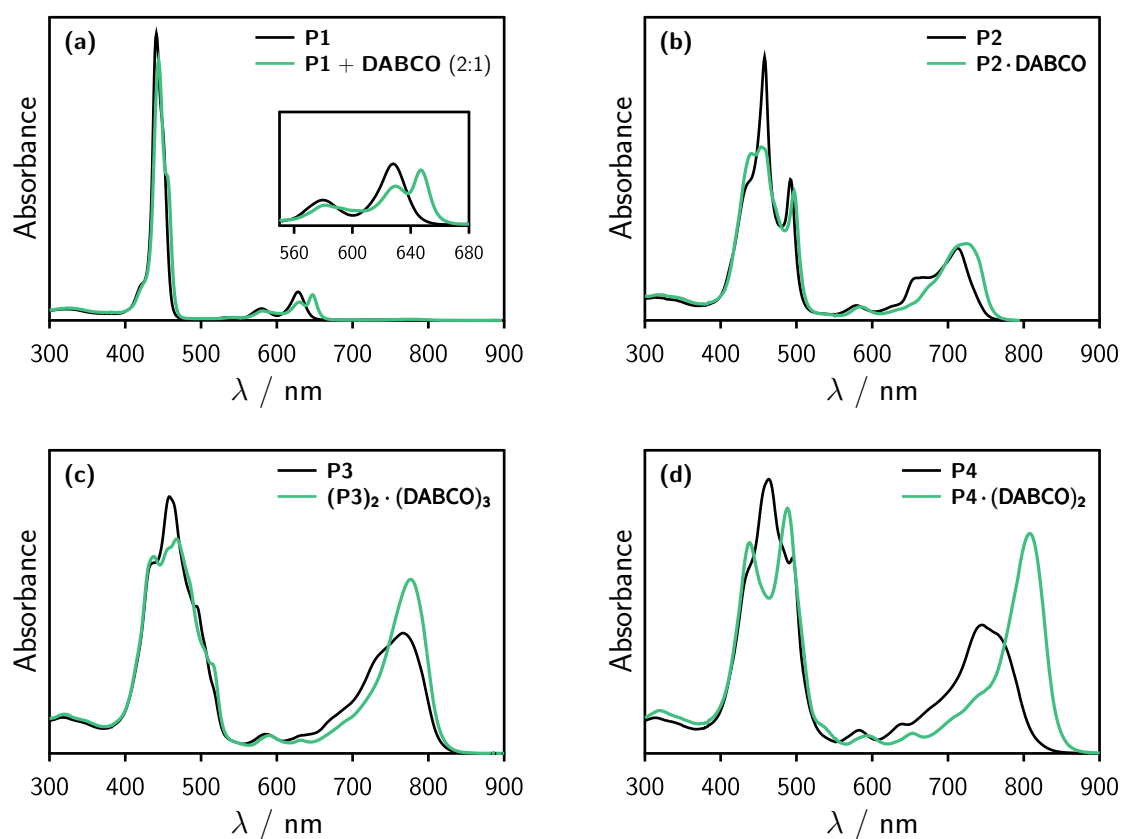


**Figure S1:** Comparison of the UV-vis absorption spectra of the linear porphyrin oligomers **P1** to **P4** in toluene solution ( $1\ \mu\text{M}$ ) and those of solutions of the linear oligomers containing the bridging ligand **DABCO** in stoichiometric equivalents for ladder formation.

However, for the longer oligomers, **P2**, **P3** and **P4**, a red-shift of the porphyrin *Q*-band is observed, along with shifts of intensity away from the blue-edge of the *Q*-band and the central peak of the porphyrin Soret band ( $\sim 450\ \text{nm}$ ) towards the red edge of the *Q*- and Soret bands. These changes are attributed to a *Q*-band red-shift resulting from axial  $\text{Zn} \cdots \text{N}$  coordination and changes in band shape arising from planarisation as a consequence of ladder formation.

When **DABCO** is added in excess, the ladder complex is found to break up again in the case of **P2** and **P3**. As has been observed before [2], the ladder complexes become gradually more stable

with increasing porphyrin oligomer length. In the case of **P4**, the stability of the ladder complex is already high enough that it cannot be broken up easily by addition of a large excess of **DABCO** and hence no further change in the UV-vis spectrum was observed once the stoichiometric point for ladder formation was reached.

## 2.2 Low Temperature UV-vis Data

Low temperature UV-vis spectra at liquid nitrogen temperatures were acquired for 1  $\mu$ M solutions of the free oligomers and ladder complexes of **P2** to **P4** in toluene and compared with the corresponding room temperature spectra in the absence and presence of **DABCO**. The results are shown in **Figures S2 and S3**. Due to the poor glass forming properties of toluene, a relatively large scattering background was present in all low temperature spectra. The spectra were background corrected using a fourth order polynomial function. The relative peak intensities might therefore not be absolutely reliable, however the prominent spectral features can clearly be distinguished and compared and were found to be well reproducible.

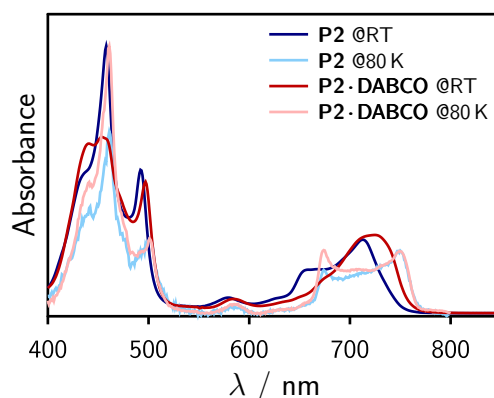


**Figure S2:** Low temperature UV-vis absorption spectra of **P2** and the corresponding ladder complex in comparison with the corresponding spectra at room temperature.

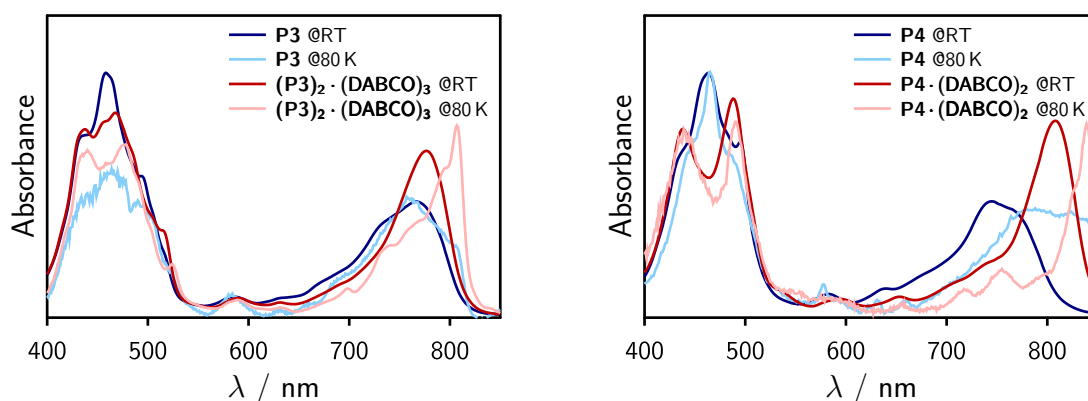


**Figure S3:** Low temperature UV-vis absorption spectra of the free oligomers and corresponding ladder complexes in comparison with the respective room temperature spectra for **P3** (left) and **P4** (right).

In the case of **P2**, the ladder complex seems to break up at low temperatures judged by the increase in intensity of the central peak of the porphyrin Soret band. In fact, the spectrum recorded at 80 K is very similar to the one recorded with an excess of **DABCO** at room temperature, suggesting a conformation where the porphyrin units within a single molecule are predominantly held at right angles with respect to each other.

For **P3** and **P4** the stability of the ladder complexes could be confirmed at low temperatures as shown in **Figure S3**. Compared to the corresponding spectra at room temperature, the ladder spectra at 80 K are red-shifted and more structured, especially in the spectral region of the porphyrin *Q* bands, but the spectral characteristics indicative for ladder formation are conserved. Low temperature spectra were also acquired in the absence of **DABCO** and show convincingly that the longer oligomers do not spontaneously adopt a co-planar conformation at low temperatures, but that the presence of **DABCO** indeed influences the geometry of the molecules at low temperature.

Since the EPR measurements were performed at higher concentrations as compared to the UV experiments ( $50\ \mu\text{M}$  vs.  $1\ \mu\text{M}$ ), it needed also to be verified that the somewhat higher concentration of the samples does not lead to a different behavior at low temperatures. For this purpose exemplary low temperature UV-vis measurements were carried out on a  $24\ \mu\text{M}$  sample of **P3** in the absence of **DABCO** in toluene. The effect of cooling on the UV-vis spectra was monitored in a temperature range between 293 and 183 K (just above the freezing point of the solvent). The obtained spectra are shown in **Figure S4** and do not show any sign of planarisation of the molecule at low temperatures, in line with the observations made at lower concentrations. This result, however, should not be regarded as a definite proof that no planarisation occurs in the free oligomers at low temperatures; it merely shows that the difference in concentration does not seem to result in major differences in the temperature dependence of the spectra.

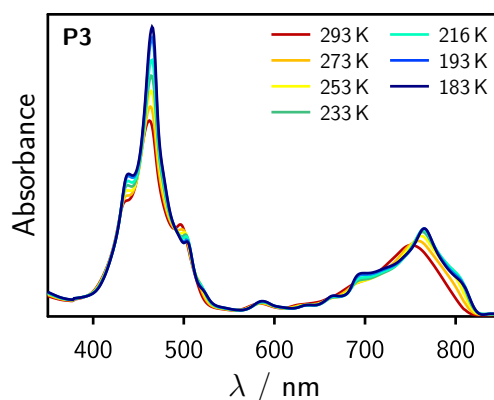


**Figure S4:** UV-vis absorption spectra of a  $24\ \mu\text{M}$  sample of **P3** at different temperatures in a range between 183 and 293 K in toluene.

### 2.3 Simulation of the TREPR Spectra

The transient cw EPR spectra of the linear oligomers **P1** to **P4** were simulated using the MATLAB software package EasySpin [3] in order to determine the zero-field splitting parameters  $D$  and  $E$  as well as the relative populations of the triplet sublevels. The best fit to the data is shown in **Figure S5** and the simulation parameters obtained are displayed in the figure. The smallest sublevel population observed for the  $Y$  sublevel was set to zero in all cases to better visualise the trends.

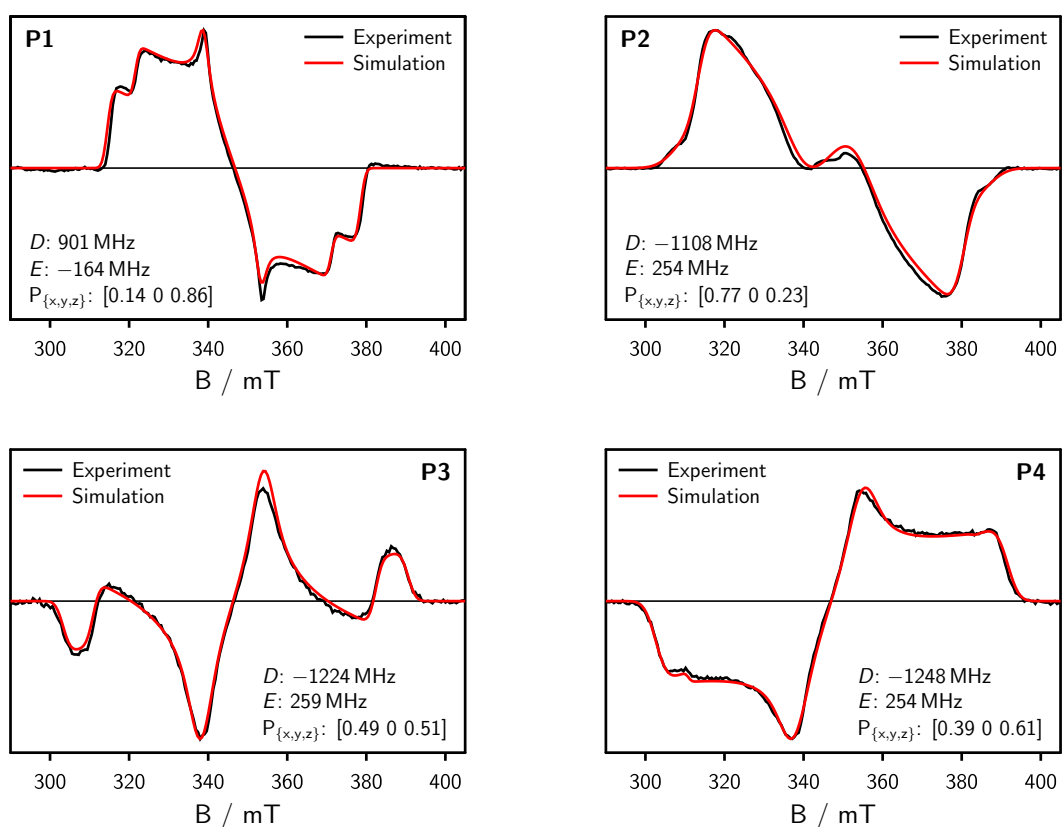


**Figure S5:** Numerical simulations of the transient cw EPR spectra of **P1** to **P4**. The simulation parameters are indicated in the figure.

As was shown before for similar systems [4], it is observed that the zero field splitting parameter  $|D|$  increases from **P1** to **P2**. Less pronounced changes in the spectral width are observed between **P2** and the longer oligomers. The relative populations obtained for the triplet sublevels deviate slightly from values reported earlier [4] by up to 20 %, presumably due to the different porphyrin side groups and the different solvent used in this work. The overall trend in all triplet state parameters, however, is identical and can be related to a gradual change in the dominant intersystem-crossing mechanism [4].

Simulations were also carried out for the transient cw EPR spectra of the ladder complexes of **P3** and **P4**. The corresponding spectra are shown in **Figure S6**. As mentioned in the main text, a slight increase in the relative in-plane triplet state sublevel populations is observed, in line with an increased planarisation of the system by comparison with the results from wavelength dependent studies where only the co-planar conformation was excited [5].

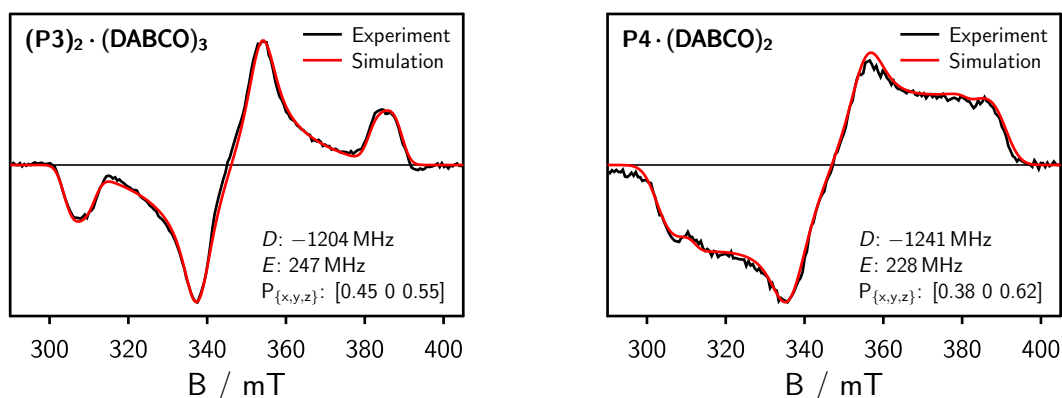


**Figure S6:** Numerical simulation of the transient cw EPR spectrum of the ladder complexes of **P3** (left) and **P4** (right) recorded at 20 K in frozen toluene. The simulation parameters are indicated in the figure.

#### 2.4 Influence of Porphyrin Side Groups

Compared to previous work [4], small differences in the triplet state parameters were observed. To confirm that these differences are due to the use of a different solvent rather than aggregation as a consequence of the smaller 3,5-bis(*tert*-butyl)phenyl (**tBu**) side groups used in this work, the spectrum of the free oligomer **P3** with 3,5-bis(trihexylsilyl)phenyl (**THS**) side groups was recorded in toluene. The result is shown in **Figure S9**. Numerical simulation yields almost identical parameters as obtained for the compound with **tBu** side groups, which should allow to exclude the possibility of aggregation.

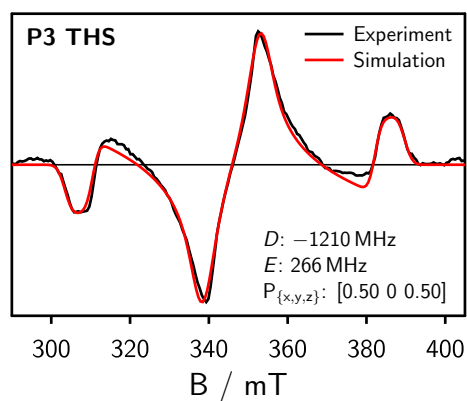


**Figure S7:** Numerical simulation of the transient cw EPR spectrum of **P3** with **THS** side groups in toluene. The simulation parameters are indicated in the figure.

### 3 DFT Calculations

Density functional theory (DFT) calculations were performed on structures of **P1** and **P2** in order to assign the experimentally determined hyperfine couplings to the nuclei and to interpret the observed trends. The orientation of the ZFS tensor and the orientation and magnitude of the proton hyperfine coupling tensors were obtained and are shown within the molecular frame in **Figure S8**.

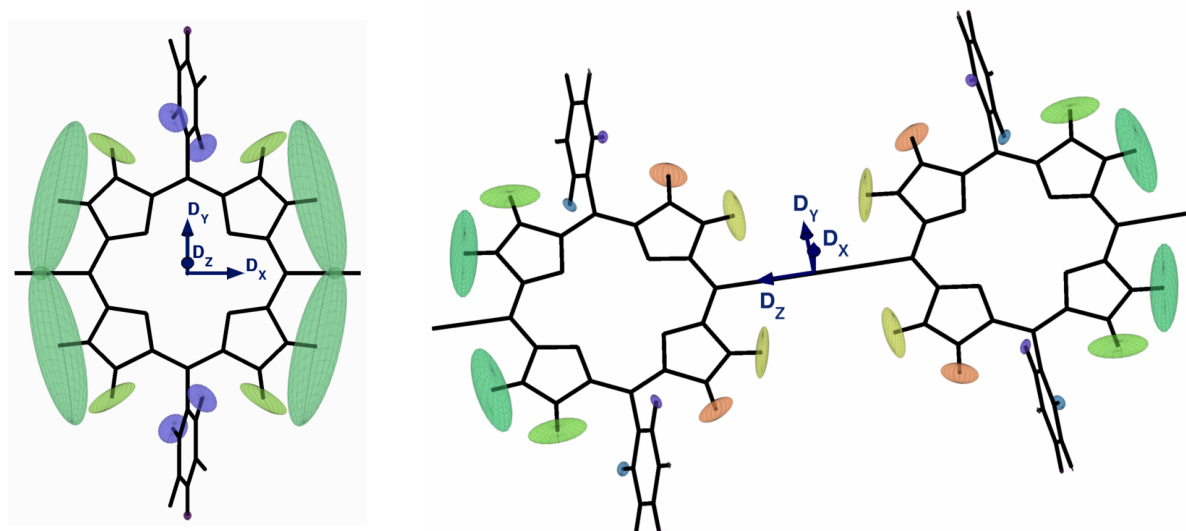


**Figure S8:** Visualisation of the zero-field splitting tensor axes and proton hyperfine interaction tensors of **P1** and **P2** in the molecular frame. Chemically equivalent  $^1\text{H}$  tensors are depicted in the same color and the size of the tensors corresponds to the relative magnitude of the hyperfine interactions. The largest hyperfine coupling of the systems used for reference in the main text is shown in dark green.

The porphyrin structures were first optimised in Turbomole V6.1 [6, 7] under  $C_1$  symmetry using DFT/B3LYP in combination with the TZVP basis set [8] and RI-approximation [9]. Frequency calculations confirmed that the obtained structures corresponded to minima of the potential energy surface. The hyperfine interaction tensors and their orientation were then calculated for the optimised structures using the program package ORCA V3.0 [10]. The ORCA DFT calculations with the B3LYP functional were performed using the EPR II basis [11] set for H, C, and N and the 6-31G basis on zinc.

## 4 Zero-Field Splitting

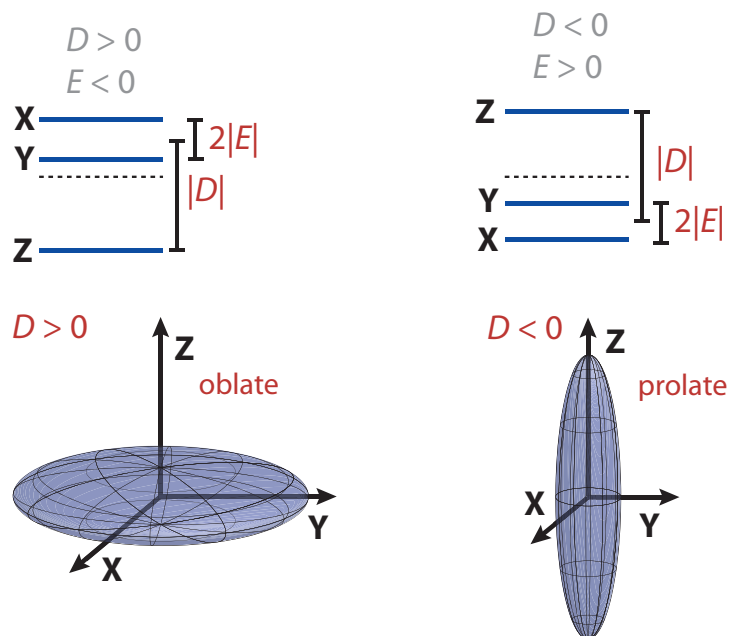


**Figure S9:** Illustration of the relative energies of the zero-field sublevels  $|X\rangle$ ,  $|Y\rangle$ , and  $|Z\rangle$  assuming  $|Z\rangle > |X\rangle > |Y\rangle$  for an oblate (**P1**) and a prolate (**P2 to P4**) system.

## References

- [1] MATLAB, *version 7.11.0 (R2010b)*; The MathWorks Inc.: Natick, Massachusetts, 2010.
- [2] Taylor, P. N.; Anderson, H. L. Cooperative Self-Assembly of Double-Stranded Conjugated Porphyrin Ladders. *J. Am. Chem. Soc.* **1999**, *121*, 11538–11545.
- [3] Stoll, S.; Schweiger, A. EasySpin, a Comprehensive Software Package for Spectral Simulation and Analysis in EPR. *J. Magn. Reson.* **2006**, *178*, 42–55.
- [4] Tait, C. E.; Neuhaus, P.; Peeks, M. D.; Anderson, H. L.; Timmel, C. R. Transient EPR Reveals Triplet State Delocalization in a Series of Cyclic and Linear pi-Conjugated Porphyrin Oligomers. *J. Am. Chem. Soc.* **2015**, *137*, 8284–8293.
- [5] Tait, C. E.; Neuhaus, P.; Peeks, M. D.; Anderson, H. L.; Timmel, C. R. Excitation Wavelength-Dependent EPR Study on the Influence of the Conformation of Multiporphyrin Arrays on Triplet State Delocalization. *Phys. Chem. Chem. Phys.* **2016**, *18*, 5275–5280.
- [6] Ahlrichs, R.; Bär, M.; Häser, M.; Horn, H.; Kölmel, C. Electronic Structure Calculations on Workstation Computers: The Program System TURBOMOLE. *Chem. Phys. Lett.* **1989**, *162*, 165–169.
- [7] TURBOMOLE V6.1 2009, a development of University of Karlsruhe and Forschungszentrum Karlsruhe GmbH, 1989-2007, TURBOMOLE GmbH, since 2007; available from <http://www.turbomole.com>.
- [8] Schäfer, A.; Huber, C.; Ahlrichs, R. Fully Optimized Contracted Gaussian Basis Sets of Triple Zeta Valence Quality for Atoms Li to Kr. *J. Chem. Phys.* **1994**, *100*, 5829–5835.
- [9] Eichkorn, K.; Weigend, F.; Treutler, O.; Ahlrichs, R. Auxiliary Basis Sets for Main Row Atoms and Transition Metals and their Use to Approximate Coulomb Potentials. *Theor. Chem. Acc.* **1997**, *97*, 119–124.
- [10] Neese, F. The ORCA Program System. *Wiley Interdiscip. Rev.: Comput. Mol. Sci.* **2012**, *2*, 73–78.
- [11] Barone, V. Structure, Magnetic Properties and Reactivities of Open-Shell Species from Density Functional and Self-Consistent Hybrid Methods. In *Recent Advances in Density Functional Methods, Part I*; Chong, D. P., Ed.; World Scientific: Singapore, 1996.